Molecular Simulation of Phase Equilibria for Water−Methane and Water−Ethane Mixtures

Jeffrey R. Errington,[†,‡] Georgios C. Boulougouris,[§,||] Ioannis G. Economou,[*,§] Athanassios Z. Panagiotopoulos,[†,‡] and Doros N. Theodorou[§,⊥]

School of Chemical Engineering, Cornell University, Ithaca, New York 14853, Institute for Physical Science and Technology and Department of Chemical Engineering, University of Maryland, College Park, Maryland 20742, Molecular Modeling of Materials Laboratory, Institute of Physical Chemistry, National Research Centre for Physical Sciences "Demokritos", GR-15310 Aghia Paraskevi Attikis, Greece, Department of Chemical Engineering, National Technical University of Athens,GR-15773 Zografos, Athens, Greece, and Department of Chemical Engineering, University of Patras, GR-26500 Patras, Greece

Received: March 25, 1998; In Final Form: August 14, 1998

Monte Carlo simulations were used to calculate water−methane and water−ethane phase equilibria over a wide range of temperatures and pressures. Simulations were performed from room temperature up to near the critical temperature of water and from subatmospheric pressure to 3000 bar. The Henry's law constants of the hydrocarbons in water were calculated from Widom test particle insertions. The Gibbs ensemble Monte Carlo method was used for simulation of the water-rich and hydrocarbon-rich phases at higher pressures. Two recently proposed pairwise additive intermolecular potentials that describe accurately the pure component phase equilibria were used in the calculations. Equations of state for associating fluids were also used to predict the phase behavior. In all cases, calculations were compared with experimental data. For the highly nonideal hydrogen bonding mixtures studied here, molecular simulation-based predictions of the mutual solubilities are accurate within a factor of 2, which is comparable with the accuracy of the best equations of state.

Introduction

The accurate knowledge of water−hydrocarbon phase equilibria and mutual solubility is important for equipment design and operation of various processes in the petroleum refining and petrochemical industry, natural and petroleum gas production, and environmental control. For many such applications, the temperature and the pressure of the system vary substantially. Several experimental studies are available in the literature,[1−4] but more data are needed, and their measurement is quite difficult and expensive. Therefore, it is highly desirable to develop predictive approaches for determining the thermodynamics of water−hydrocarbon mixtures over a wide range of conditions.

Molecular simulation techniques developed over the past decade allow direct calculation of mixture phase equilibria.[5−8] The most widely used method is Gibbs ensemble Monte Carlo (GEMC), which is based on simultaneous simulation of the phases at equilibrium and "jumps" of molecules between the phases so that the chemical potential of each species is statistically the same in all phases.[5] This method is used here for the high-pressure phase equilibrium simulations.

To ensure a quantitative agreement between simulation and experimental data, adequate molecular potentials are needed for the various species involved. Most of the semiempirical two-body molecular potentials available in the literature for water were developed to reproduce accurately thermodynamic and structural properties over a relatively narrow temperature range (20−40 °C).[9−11] These models consist of a Lennard-Jones sphere located on the oxygen atom and partial charges located on the hydrogen atoms and on or near the oxygen atom. Recently, Boulougouris et al.[12] used the simplified point charge (SPC) and extended-SPC (SPC/E) models to simulate the phase equilibria and other thermodynamic (such as second virial coefficient and heat of vaporization) and structural (such as radial distribution function) properties of pure water from 300 K to 600 K. They showed that agreement with experimental data at subcritical conditions improves substantially by reparametrization of the SPC/E model into a modified-SPC/E (MSPC/E) model. However, the MSPC/E model does not reproduce the critical parameters of water, which could result in inaccurate prediction of the phase equilibria at increased temperatures and pressures. Errington and Panagiotopoulos[13] proposed a modified Buckingham exponential-6 potential (hereafter called exp-6) to account for the nonpolar interactions in water. The new model predicts accurately the coexisting densities, vapor pressure, and critical properties of water.

Substantial work has been done over the past few years on developing transferable potentials for phase equilibrium calculations of *n*-alkanes, from methane to heavy hydrocarbons, such as octatetracontane (nC_{48}).[14−16] These models utilize a united-atom representation in which hydrogens are not taken into account explicitly and energetic interactions are calculated through the Lennard-Jones potential. The models provide generally good agreement with experimental phase coexistence data, including the critical region.

* Author for correspondence. Fax ++3016511766; E-mail economou@cyclades.nrcps.ariadne-t.gr.
† Cornell University.
‡ University of Maryland.
§ National Research Centre for Physical Sciences.
|| National Technical University of Athens.
⊥ University of Patras.

10.1021/jp981627v CCC: $15.00
Published on Web 10/13/1998

TABLE 1: Parameter Values for the Molecular Models Examined in This Work

	Water			Methane		Ethane	
model parameter	SPC/E	MSPC/E	exp-6	TraPPE	exp-6	TraPPE	exp-6
ϵ/k_B (K)	78	74.5	159.8	148	160.3	98	129.6
σ (Å)	3.166	3.116	3.1947	3.73	3.741	3.75	3.679
α			12		15		16
R_{OH} (Å)	1.0	0.9839	1.0668				
HOH angle (deg)	109.47	109.47	109.47				
q (esu)	0.4238	0.4108	0.3687				
C−C bond length (Å)						1.54	1.839

The focus of this work is on the phase behavior of binary mixtures of water with methane or ethane. More specifically, Monte Carlo simulations were performed to calculate the Henry's law constant of the two hydrocarbons in water over a wide temperature range (300−570 K) close to the saturation curve of pure water. Henry's law provides a convenient description of the solubility of hydrocarbons in water at low and moderate pressure. Calculations were performed using the SPC/E and the MSPC/E model for pure water, whereas methane and ethane were modeled using the transferable potentials for phase equilibrium (TraPPE) model.[16] In addition, GEMC simulation was used to calculate the high-pressure phase equilibria for the two mixtures. In this case, two different types of potentials were used. In the first set of simulations, the MSPC/E model was used for water and the TraPPE model for the two hydrocarbons, whereas in the second set of simulations, the exp-6 model was used for all three components. As a result, a direct comparison can be made concerning the accuracy of the different types of molecular potentials for mixture phase equilibria. In all cases, simulations are compared against experimental data from the literature.[17−19]

In engineering applications, it is desirable to have an accurate closed-form model for phase equilibrium calculations, such as an equation of state (EoS). In this work, two state-of-the-art EoS for associating fluids, the associated perturbed anisotropic chain theory[20] (APACT) and the statistical associating fluid theory[21] (SAFT), are used for the high-pressure water−methane and water−ethane phase equilibria. Calculations were performed without the use of any binary adjustable parameter, so that these macroscopic EoS predictions are used in "predictive" mode to provide a basis for comparisons with molecular simulation results.

Intermolecular Potential Models

Most of the simple two-body potentials developed for water are variations of the Bernal and Fowler model.[22] Water is modeled as a Lennard-Jones sphere located on the oxygen atom, two positive partial charges located on the hydrogen atoms, and one negative partial charge located either on the oxygen atom (three-site models) or on the dichotomy of H−O−H angle (four-site models). In this work, two three-site models were used for water, namely the SPC/E[11] and the MSPC/E.[12] Both models have the same functional form given by the equation:

$$u(r) = 4\epsilon\left[\left(\frac{\sigma}{r}\right)^{12} - \left(\frac{\sigma}{r}\right)^{6}\right] + \sum_{\gamma=1}^{3}\sum_{\delta=1}^{3}\frac{q_\gamma q_\delta}{r_{\gamma\delta}} \qquad (1)$$

where the indices γ and δ run over all charges on the molecules. In Table 1, the values for ϵ (interaction energy), σ (Lennard-Jones sphere diameter), and q (hydrogen partial charge) are shown for the two models together with the geometric characteristics of the models (the O−H distance, R_{OH}, and the H−O−H angle).

Methane and ethane molecules are modeled with a united-atom Lennard-Jones representation. In this work, the TraPPE parameter set[16] was used. In Table 1, these parameters are shown for the two hydrocarbons. The standard Lorentz−Berthelot combining rules were used for the interactions between unlike molecules:

$$\epsilon_{ij} = \sqrt{\epsilon_{ii}\epsilon_{jj}} \qquad (2)$$

$$\sigma_{ij} = \frac{\sigma_{ii} + \sigma_{jj}}{2} \qquad (3)$$

Furthermore, calculations were performed using the exp-6 model[23] for water, methane, and ethane. The functional form of this model is slightly more complicated than the Lennard-Jones model and is given by the expression:

$$u(r) = \begin{cases} \dfrac{\epsilon}{1 - 6/\alpha}\left[\dfrac{6}{\alpha}\exp\left(\alpha\left[1 - \dfrac{r}{r_m}\right]\right) - \left(\dfrac{r_m}{r}\right)^6\right], & \text{for } r > r_{max} \\ \infty & \text{for } r < r_{max} \end{cases} \qquad (4)$$

In the case of water, a coulombic term is added to the potential, similar to eq 1. In eq 4, r_m is the radial distance at which the potential has a minimum, r_{max} is the smallest positive value for which $du(r)/dr = 0$, and σ (not shown explicitly in eq 4) is the point at which $u(r) = 0$. The parameters r_m and r_{max} can be expressed in terms of ϵ, σ, and α. Errington and Panagiotopoulos[13] calculated an optimum set of ϵ, σ, and α parameters for water (optimum q and R_{OH} values were also obtained), methane, and ethane (optimum C−C bond length was also obtained) by fitting the coexisting densities, vapor pressure, and critical constants of the components. In Table 1, ϵ, σ, and α values are shown for the three components. The C−C bond length in the exp-6 model is ∼20% longer than the experimentally measured bond length. This value was used for other potential models for ethane and was shown to provide an accurate prediction of the pure component phase equilibrium properties.[24] Interactions between unlike molecules are calculated through the Lorentz−Berthelot combining rules given by eqs 2 and 3 and the expression:

$$\alpha_{ij} = \sqrt{\alpha_{ii}\alpha_{jj}} \qquad (5)$$

Theory

The Henry's law constant of a solute (methane or ethane in this case) in water ($H_{hc\to w}$) is given from the expression:[25]

$$H_{hc\to w} = \lim_{x_{hc}\to 0}\left(\frac{f_{hc}}{x_{hc}}\right) \qquad (6)$$

where x_{hc} is the mole fraction and f_{hc} the fugacity of the hydrocarbon. Using standard thermodynamic relations, eq 6 can be written as:

$$H_{hc\rightarrow w} = \lim_{x_{hc}\rightarrow 0}\left(\frac{\rho_w}{\beta}\exp(\beta\mu_{hc}^{ex})\right) \quad (7)$$

where ρ_w is the pure water number density at a given temperature (T) and pressure (P), $\beta = 1/k_BT$, and μ_{hc}^{ex} is the hydrocarbon excess chemical potential in water at these conditions. The excess chemical potential of a species in a mixture is defined as the chemical potential of the species at a given temperature, density, and composition minus the ideal gas chemical potential of the pure species at the temperature and molecular density it has in the mixture. This calculation of μ_{hc}^{ex} is usually performed by using the Widom test particle insertion method,[26] and in this case a hydrocarbon test particle (methane or ethane) was inserted in pure water. Simulations were performed in the *NPT* (isobaric−isothermal) ensemble and μ_{hc}^{ex} was evaluated from the expression:[27]

$$\mu_{hc}^{ex} = -k_BT\ln\left[\frac{1}{\langle V\rangle_{NPT}}\langle V\langle\exp(-\nu_{test}/k_BT)\rangle_{Widom,NV}\rangle_{NPT}\right] \quad (8)$$

where ν_{test} is the total energy on the test molecule by the water molecules of the system.

Simulation Details

To calculate the Henry's law constant of methane and of ethane in water, pure liquid water was simulated initially in the *NPT* ensemble. A constant number of 250 water molecules was equilibrated for (20−100) × 10^6 moves (depending on the temperature) and then another (40−80) × 10^6 moves were performed where thermodynamic properties were averaged. Particle displacement and rotation and volume fluctuation were used according to the ratio: 99.6% particle displacement and rotation and 0.4% volume fluctuation. From each simulation, ~300 configurations were stored and used subsequently to evaluate the hydrocarbon μ_{hc}^{ex}. Since the MSPC/E model was developed on the basis of the SPC/E model by using scaling concepts,[12] calculations with the two models at the same reduced thermodynamic conditions were performed with a single configuration file produced from one *NPT* run.

In postprocessing, (4−40) × 10^3 hydrocarbon molecule insertions were attempted for each configuration. At the lowest end of the temperature range examined, the highest number of insertions was performed, whereas for temperatures >470 K, 4000 insertions were sufficient to provide a reliable estimate of μ_{hc}^{ex}. The block averaging technique was used to calculate statistical uncertainties and each run was divided into five blocks. The cutoff radius for water−water Lennard-Jones interactions was 2.5σ, whereas for water-hydrocarbon interactions it was 2.75σ. This small difference in the truncation distance has no effect in the final results. Especially for water−water interactions, the dominant effects are taken into account through the Ewald summation method.

For the calculation of high-pressure water−methane and water−ethane, GEMC simulations were performed. Most of the simulations were done for constant temperature, pressure, and total number of molecules (GEMC−*NPT* simulation). For a few cases in the vicinity of water critical point where GEMC−*NPT* simulations were unstable, calculations were performed for constant temperature, total volume, and total number of molecules (GEMC−*NVT* simulation). Configurational bias sampling methods[28−30] were used to enhance the efficiency of the transfer moves. A typical system consisted of 300 molecules (~200 water and 100 hydrocarbon molecules) placed in the two boxes with a composition near the experimental composition, and density near that of pure water and hydrocarbon, respectively, at the same conditions. An initial equilibration period of 2 × 10^6 moves was followed by 6 × 10^6 moves where thermodynamic properties were averaged. The ratio of the different moves used in the calculations was: 50% particle displacement, 34% particle rotation, 1% volume fluctuation, and 15% particle transfer between the boxes. Statistical uncertainties were calculated using the block averaging technique, with each run divided into five blocks. The method of Theodorou and Suter[31] was used for the nonpolar long-range corrections.

For all the simulations, the full Ewald summation method was used to account for the long-range coulombic interactions. Details concerning the implementation of the Ewald summation method are given elsewhere.[12,27]

Equations of State

Two semitheoretical EoS for associating fluids[20,21] (APACT and SAFT) were used for the prediction of high-pressure phase equilibria. Both EoS account explicitly for repulsive interactions, dispersive van der Waals interactions, and hydrogen bonding. In addition, APACT accounts explicitly for polar (dipolar and quadrupolar) and induced dipolar interactions. The functional form of both EoS is quite similar, and in terms of the compressibility factor, $Z = P\upsilon/RT$, is

$$Z = 1 + Z^{rep} + Z^{att} + Z^{assoc} \quad \text{(APACT)} \quad (9)$$

$$Z = 1 + Z^{seg} + Z^{chain} + Z^{assoc} \quad \text{(SAFT)} \quad (10)$$

Detailed expressions for the different terms of the EoS can be found elsewhere[21,32,33] and are not repeated here. In this work, water was modeled with APACT as a three-hydrogen bonding site species (two proton donor sites and one proton acceptor site), and in SAFT as a four-site species (two proton donor sites and two proton acceptor sites). The effect of the number of hydrogen bonding sites on the phase equilibria of water−hydrocarbon mixtures has been examined previously.[34] The EoS parameters were taken from Economou and Tsonopoulos[34] for water for both APACT and SAFT, and from Huang and Radosz[21] for SAFT and Vimalchand et al.[35] for APACT for the case of methane and ethane. No binary interaction parameter was adjusted to the experimental data, so that predictions from these EoS are directly comparable with simulation results.

Results and Discussion

Henry's Law Constants. The Henry's law constant is a convenient measure of the usually small solubilities of hydrocarbons in water, especially at low and intermediate temperature and pressure. For low solubility values, Henry's law constant is inversely proportional to the solubility, x_{hc}, according to the expression:[25]

$$H_{hc\rightarrow water} \propto \lim_{x_{hc}\rightarrow 0}\left(\frac{P}{x_{hc}}\right) \quad (11)$$

Simulation results and a very accurate empirical correlation of the experimental data[19] for the Henry's law constant of methane and of ethane in water are shown in Table 2 (for the SPC/E model) and Table 3 (for the MSPC/E model) and are plotted in Figure 1 (for methane) and Figure 2 (for ethane). Calculations at the same pure water-based reduced conditions using the SPC/E and MSPC/E were performed in a single simulation, and by using scaling concepts the actual thermo-

TABLE 2: Liquid Density of Pure Water and Henry's Law Constant of Methane and Ethane in Water (*NPT* Monte Carlo Simulation with the Widom Test Particle Insertion Technique[26] Using the SPC/E Model for Water and the TraPPE Model for Methane and Ethane, and Experimental Data[19])

		water liquid density (g/cm^3)	methane Henry's constant (kbar)		ethane Henry's constant (kbar)	
temperature (K)	pressure (bar)	simulation	simulation	experimental	simulation	experimental
314.1	0.02	0.988 ± 0.003	46 ± 7	50	25 ± 9	43
348.7	0.14	0.961 ± 0.004	55 ± 7	63	58 ± 15	64
390.7	0.80	0.934 ± 0.002	68 ± 7	62	70 ± 16	66
423.2	3.04	0.898 ± 0.006	54 ± 5	53	62 ± 10	55
470.1	10.00	0.835 ± 0.004	36 ± 5	36	42 ± 9	34
492.3	14.96	0.792 ± 0.008	27 ± 6	29	29 ± 10	26
500.0	18.00	0.789 ± 0.005	25 ± 3	27	28 ± 5	23
556.5	49.86	0.680 ± 0.013	12 ± 1	14	12 ± 1	10
570.0	65.00	0.652 ± 0.013	10 ± 1	12	10 ± 2	8

TABLE 3: Liquid Density of Pure Water and Henry's Law Constant of Methane and Ethane in Water (*NPT* Monte Carlo Simulation with the Widom Test Particle Insertion Technique[26] Using the MSPC/E Model for Water and the TraPPE Model for Methane and Ethane, and Experimental Data[19])

		water liquid density (g/cm^3)	methane Henry's constant (kbar)		ethane Henry's constant (kbar)	
temperature (K)	pressure (bar)	simulation	simulation	experimental	simulation	experimental
300.0	0.02	1.038 ± 0.004	44 ± 8	41	23 ± 8	31
333.0	0.14	1.010 ± 0.004	55 ± 7	59	57 ± 19	56
373.0	0.80	0.981 ± 0.003	69 ± 8	64	67 ± 18	69
404.1	3.05	0.943 ± 0.006	54 ± 5	59	61 ± 11	63
449.0	10.03	0.877 ± 0.005	37 ± 5	44	42 ± 10	43
470.1	15.00	0.832 ± 0.009	27 ± 6	36	29 ± 10	34
477.5	18.05	0.829 ± 0.005	25 ± 3	34	28 ± 5	31
531.5	50.00	0.714 ± 0.014	12 ± 1	19	12 ± 1	15
544.4	65.18	0.685 ± 0.014	10 ± 1	16	10 ± 2	12

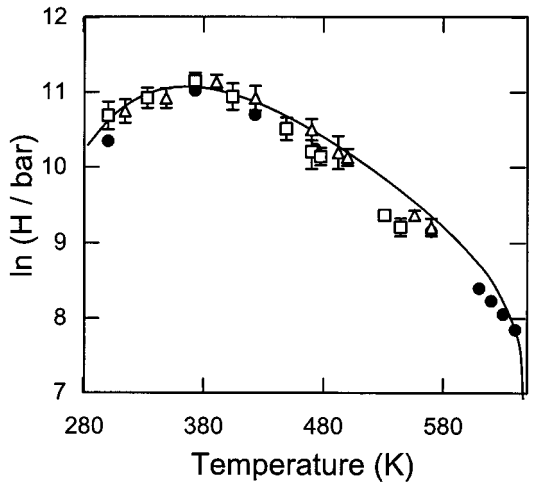

Figure 1. Henry's law constant of methane in water. Experimental data (solid line),[19] Monte Carlo simulations using the SPC/E (open triangles) and MSPC/E (open squares) models for water and the TraPPE model for methane calculated in this work, and molecular dynamics results (filled circles) from Guillot and Guissani.[36]

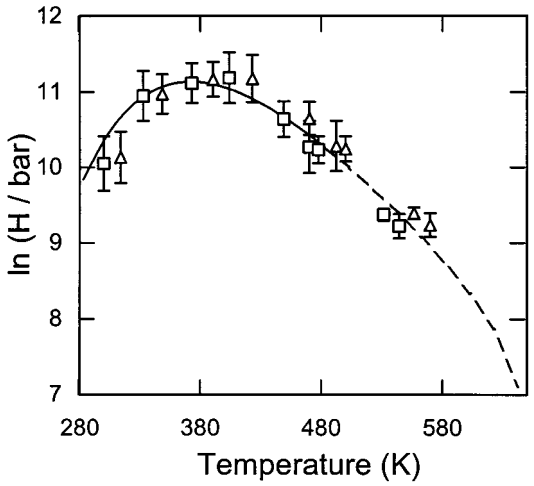

Figure 2. Henry's law constant of ethane in water. Experimental data (solid line),[19] and Monte Carlo simulations using the SPC/E (open triangles) and MSPC/E (open squares) models for water and the TraPPE model for ethane calculated in this work. The dashed line is an extrapolation of the correlation proposed by Harvey.[19]

dynamic properties were obtained.[12] The empirical correlation for ethane was fitted to experimental data up to 473 K; for higher temperature the same correlation is shown as a dashed line in Figure 2. Although both SPC/E and MSPC/E models are in good agreement with the experiment, the MSPC/E model is consistently closer to the experimental data up to 450 K. This is due to the fact that the MSPC/E model is more accurate for the pure water phase equilibrium than SPC/E.[12] For higher temperatures, MSPC/E predictions are systematically lower than the experimental data and the SPC/E predictions, because the MSPC/E critical temperature is 602 K compared with the experimental value of 647.1 K and the SPC/E value of 635 ± 5 K[12] During the Widom insertion process, ethane molecules are relatively more difficult to be inserted in an energetically favorable position and so the estimated Henry's constant has a larger statistical error than the Henry's constant for methane.

It is remarkable that both models capture accurately the maximum value for $H_{hc\rightarrow water}$ at ~373 K, which, in turn, corresponds to a minimum in the solubility. The maximum value for $H_{hc\rightarrow water}$ is the combined effect of enthalpic and entropic contributions and is a characteristic of all the hydrocarbons dissolved in water.[1,2,4] According to Guillot and Guissani,[36] water at relatively low temperatures forms cavities as a result of the strong hydrogen bonding, and so the solubility of small dissolved molecules increases as the temperature decreases (entropic effect). As the temperature increases above ~450 K, hydrogen bonding networks break down, allowing hydrocarbon molecules to penetrate into the aqueous phase and thus hydrocarbon solubility increases again. EoS for associating

TABLE 4: Phase Equilibria for Water−Methane (GEMC Simulation Using the MSPC/E Model for Water and the TraPPE Model for Methane)

		liquid phase		vapor phase	
temperature (K)	pressure (bar)	methane mole fraction	density (g/cm^3)	water mole fraction	density (g/cm^3)
423	100	0.0010 ± 0.0005	0.94 ± 0.02	0.044 ± 0.011	0.047 ± 0.001
423	250	0.0021 ± 0.0007	0.95 ± 0.01	0.015 ± 0.003	0.113 ± 0.001
423	500	0.0037 ± 0.0014	0.97 ± 0.02	0.008 ± 0.001	0.194 ± 0.002
423	1000	0.0028 ± 0.0005	1.00 ± 0.01	0.005 ± 0.001	0.278 ± 0.002
523	100	0.0016 ± 0.0004	0.81 ± 0.01	0.562 ± 0.009	0.048 ± 0.001
523	250	0.008 ± 0.003	0.79 ± 0.03	0.23 ± 0.06	0.096 ± 0.005
523	500	0.011 ± 0.004	0.82 ± 0.02	0.12 ± 0.04	0.162 ± 0.003
523	1000	0.014 ± 0.003	0.85 ± 0.01	0.05 ± 0.02	0.243 ± 0.002
603	1000	0.07 ± 0.02	0.65 ± 0.04	0.22 ± 0.06	0.240 ± 0.013

TABLE 5: Phase Equilibria for Water−Methane (GEMC Simulation Using the Exp-6 Model for Water and for Methane)

		liquid phase		vapor phase	
temperature (K)	pressure (bar)	methane mole fraction	density (g/cm^3)	water mole fraction	density (g/cm^3)
423	100	0.0008 ± 0.0003	0.911 ± 0.004	0.054 ± 0.009	0.047 ± 0.001
423	250	0.0015 ± 0.0003	0.919 ± 0.004	0.026 ± 0.003	0.113 ± 0.001
423	500	0.0025 ± 0.0012	0.933 ± 0.010	0.017 ± 0.003	0.194 ± 0.002
423	1000	0.0033 ± 0.0010	0.951 ± 0.005	0.0092 ± 0.0008	0.278 ± 0.003
523	100	0.0013 ± 0.0004	0.803 ± 0.012	0.50 ± 0.03	0.044 ± 0.002
523	250	0.005 ± 0.002	0.797 ± 0.012	0.23 ± 0.03	0.094 ± 0.002
523	500	0.010 ± 0.001	0.801 ± 0.006	0.13 ± 0.02	0.164 ± 0.002
523	1000	0.017 ± 0.004	0.828 ± 0.013	0.07 ± 0.01	0.245 ± 0.004
603	294 ± 19	0.020 ± 0.005	0.621 ± 0.028	0.60 ± 0.04	0.128 ± 0.012
603	491 ± 8	0.028 ± 0.004	0.656 ± 0.015	0.52 ± 0.06	0.199 ± 0.022
603	1000	0.040 ± 0.002	0.707 ± 0.005	0.35 ± 0.07	0.268 ± 0.020

TABLE 6: Phase Equilibria for Water−Ethane (GEMC Simulation Using the MSPC/E Model for Water and the TraPPE Model for Ethane)

		liquid phase		vapor phase	
temperature (K)	pressure (bar)	ethane mole fraction	density (g/cm^3)	water mole fraction	density (g/cm^3)
523	200	0.004 ± 0.001	0.78 ± 0.01	0.25 ± 0.04	0.138 ± 0.005
523	500	0.008 ± 0.002	0.82 ± 0.01	0.074 ± 0.009	0.298 ± 0.006
523	1000	0.007 ± 0.002	0.87 ± 0.01	0.033 ± 0.004	0.400 ± 0.002
523	1500	0.007 ± 0.004	0.91 ± 0.01	0.024 ± 0.007	0.454 ± 0.001
523	2000	0.005 ± 0.002	0.95 ± 0.01	0.019 ± 0.005	0.490 ± 0.001
523	3000	0.003 ± 0.001	1.00 ± 0.01	0.015 ± 0.008	0.539 ± 0.002
573	500	0.018 ± 0.006	0.71 ± 0.03	0.29 ± 0.04	0.269 ± 0.006
573	1000	0.015 ± 0.002	0.79 ± 0.01	0.10 ± 0.01	0.375 ± 0.004
573	1500	0.014 ± 0.004	0.84 ± 0.01	0.06 ± 0.01	0.434 ± 0.002
573	2000	0.011 ± 0.001	0.88 ± 0.01	0.05 ± 0.02	0.472 ± 0.001
573	3000	0.009 ± 0.002	0.94 ± 0.01	0.03 ± 0.01	0.524 ± 0.001

fluids are incapable of predicting this behavior (they predict that the solubility of hydrocarbons in water is a monotonic function of temperature[34]), and so the calculations presented here show a clear advantage of molecular-based calculations over more macroscopic approaches.

In Figure 1, calculations from molecular dynamics simulation[36] using the SPC/E model for water and a model for methane that is very close to the TraPPE model are plotted. These results are in good agreement with our Monte Carlo simulation at temperatures well below the water critical temperature, given the statistical uncertainty in the calculations. It is well known[37,38] that for any solute i dissolved in a solvent j in the vicinity of the solvent critical temperature, $T_{c,j}$:

$$\lim_{T\to T_{c,j}} \frac{\partial(H_i/\phi_i^{\infty})}{\partial T} = -\infty \qquad (12)$$

where ϕ_i^{∞} is the fugacity coefficient of solute i at infinite dilution at the solvent critical point. Because ϕ_i^{∞} has a finite value at $T_{c,j}$,[25] H_i diverges to satisfy eq 12. Given that the water critical temperature for the SPC/E model is 635 ± 5 K,[12] Guillot and Guissani[36] results for the temperature dependence of H_i in the vicinity of the water critical temperature seem not to exhibit the correct slope.

High-Pressure Phase Equilibria. As the pressure increases, considerable deviations from Henry's law are observed and so mutual solubilities are needed. The high-pressure water−methane and water−ethane phase equilibrium results calculated in this work are shown in Tables 4 through 7 and Figures 3 through 8. The SPC/E model was not used for these calculations, because the MSPC/E model was proven more accurate for both the pure water phase equilibrium and the Henry's constant of methane and ethane in water at temperatures below the pure water critical temperature. Instead, calculations using the exp-6 model are shown for both systems. Finally, predictions from the two EoS, APACT and SAFT, are included for comparison. The high-pressure hydrocarbon solubility in water can be used in eq 11 to obtain an estimate of the Henry's constant pressure dependence.

The MSPC/E−TraPPE predictions for methane solubility in water are in very good agreement with the experimental data[18] at 423 and 523 K, especially at pressures up to 500 bar. For these conditions, the exp-6 model predicts lower methane solubility in water. For the case of water solubility in methane,

TABLE 7: Phase Equilibria for Water−Ethane (GEMC Simulation Using the Exp-6 Model for Water and for Ethane)

		liquid phase		vapor phase	
temperature (K)	pressure (bar)	ethane mole fraction	density (g/cm^3)	water mole fraction	density (g/cm^3)
523	200	0.0032 ± 0.0006	0.792 ± 0.005	0.29 ± 0.03	0.143 ± 0.004
523	500	0.006 ± 0.001	0.813 ± 0.009	0.15 ± 0.04	0.297 ± 0.003
523	1000	0.006 ± 0.001	0.844 ± 0.003	0.08 ± 0.02	0.392 ± 0.002
523	1500	0.008 ± 0.002	0.867 ± 0.007	0.052 ± 0.006	0.441 ± 0.003
523	2000	0.006 ± 0.002	0.899 ± 0.008	0.05 ± 0.02	0.476 ± 0.002
523	3000	0.007 ± 0.005	0.93 ± 0.01	0.03 ± 0.02	0.524 ± 0.003
573	500	0.02 ± 0.01	0.72 ± 0.03	0.34 ± 0.08	0.276 ± 0.011
573	1000	0.019 ± 0.005	0.77 ± 0.01	0.18 ± 0.01	0.373 ± 0.001
573	1500	0.015 ± 0.003	0.81 ± 0.01	0.13 ± 0.03	0.427 ± 0.003
573	2000	0.015 ± 0.006	0.84 ± 0.01	0.10 ± 0.01	0.459 ± 0.002
573	3000	0.013 ± 0.007	0.89 ± 0.01	0.07 ± 0.02	0.509 ± 0.001
623	241 ± 12	0.009 ± 0.002	0.59 ± 0.02	0.87 ± 0.03	0.179 ± 0.028
623	438 ± 9	0.06 ± 0.02	0.54 ± 0.04	0.63 ± 0.06	0.255 ± 0.023
623	471 ± 7	0.06 ± 0.03	0.56 ± 0.05	0.63 ± 0.03	0.270 ± 0.011
623	1077 ± 14	0.07 ± 0.02	0.64 ± 0.03	0.38 ± 0.04	0.381 ± 0.009
623	1250 ± 35	0.04 ± 0.02	0.72 ± 0.04	0.43 ± 0.12	0.413 ± 0.029
623	1500	0.04 ± 0.03	0.72 ± 0.04	0.26 ± 0.08	0.414 ± 0.007
623	2000	0.05 ± 0.02	0.75 ± 0.02	0.21 ± 0.11	0.453 ± 0.011

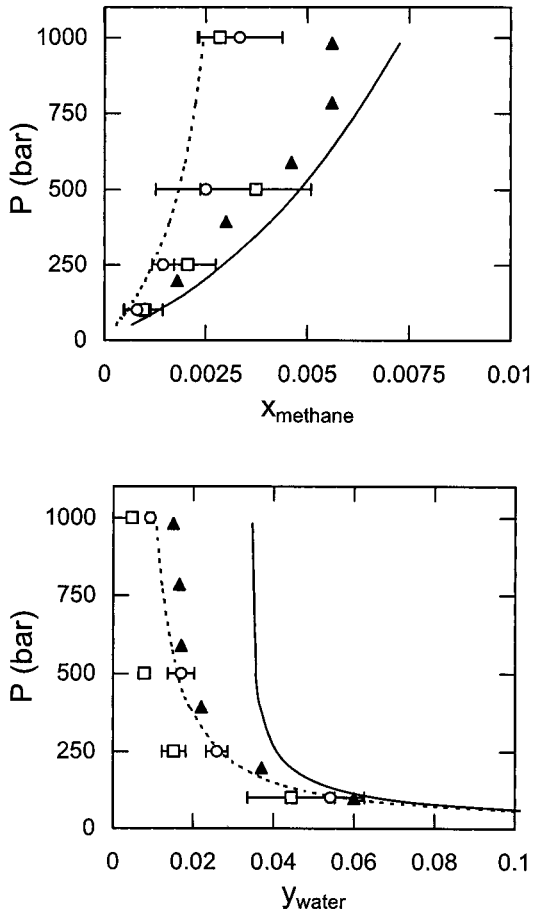

Figure 3. Water−methane high-pressure phase equilibria at 423 K (top: liquid-phase composition; bottom: vapor-phase composition). Experimental data (solid triangles),[18] GEMC simulation with the MSPC/E−TraPPE model (open squares) and with the exp-6 model (open circles), and EoS predictions from APACT (dashed lines) and SAFT (solid lines).

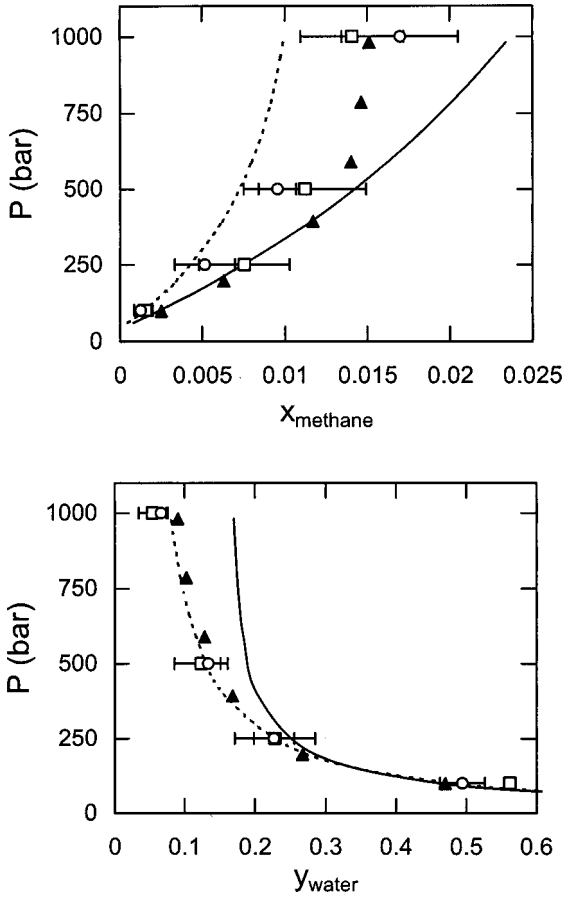

Figure 4. Water−methane high-pressure phase equilibria at 523 K (top: liquid-phase composition; bottom: vapor-phase composition). Experimental data (solid triangles),[18] GEMC simulation with the MSPC/E−TraPPE model (open squares) and with the exp-6 model (open circles), and EoS predictions from APACT (dashed lines) and SAFT (solid lines).

the exp-6 model is consistently superior to the MSPC/E−TraPPE model and in close agreement with the experimental data. At the highest temperature examined (603 K), the exp-6 predictions are in reasonably good agreement with experimental data over the entire pressure range (300−1000 bar). On the other hand, the water critical temperature for the MSPC/E model is 602 K[12] and as a result the mixture simulation with this model was unstable at this temperature. The only stable calculations were obtained for the highest pressure examined at 1000 bar where the statistical uncertainty for the methane composition was very large compared with the exp-6 simulation. The exp-6 model prediction for the water critical temperature almost coincides with the experimental value,[13] and this accuracy is reflected on the mixture calculations presented here at 603 K.

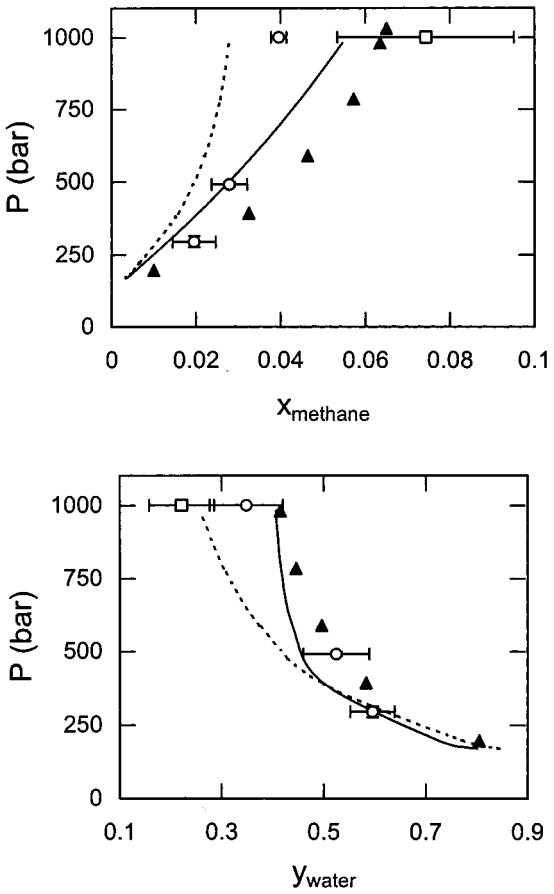

Figure 5. Water−methane high-pressure phase equilibria at 603 K (top: liquid-phase composition; bottom: vapor-phase composition). Experimental data (solid triangles),[18] GEMC simulation with the MSPC/E−TraPPE model (open squares) and with the exp-6 model (open circles), and EoS predictions from APACT (dashed lines) and SAFT (solid lines).

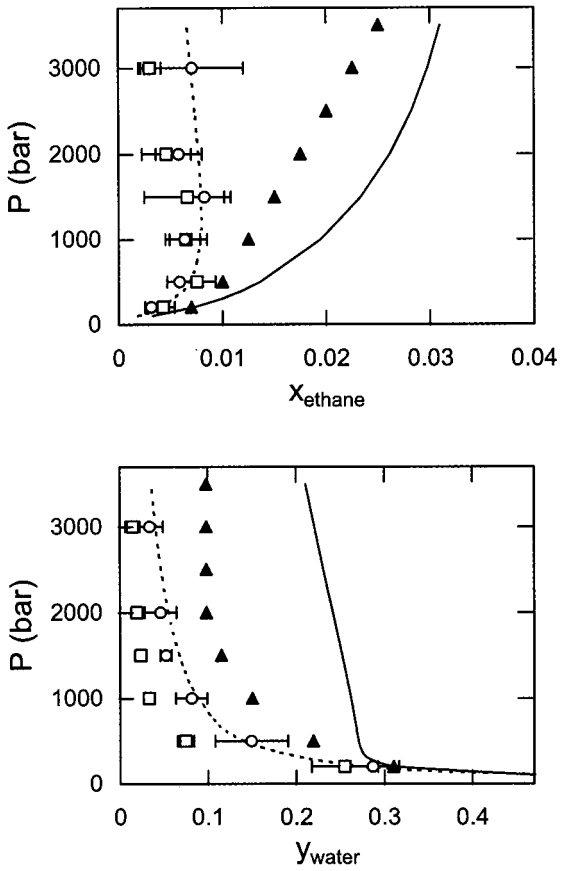

Figure 6. Water−ethane high-pressure phase equilibria at 523 K (top: liquid-phase composition; bottom: vapor-phase composition). Experimental data (solid triangles),[17] GEMC simulation with the MSPC/E−TraPPE model (open squares) and with the exp-6 model (open circles), and EoS predictions from APACT (dashed lines) and SAFT (solid lines).

SAFT predictions for methane solubility in water are in good agreement with the experimental data at 423 K and 523 K and for pressures up to ∼500 bar. For higher pressures, SAFT predicts that methane solubility increases with increasing pressure, whereas experimental data (and APACT predictions) show that a plateau is reached at ∼750 bar. APACT predicts lower methane solubility than the experimental data, but is very accurate for the prediction of water solubility in methane at 423 K and 523 K. The water solubility predicted by SAFT is almost twice the experimental value at 423 K and 523 K and relatively high pressure. Finally, at 603 K, SAFT is more accurate than APACT for the composition in both phases.

The water−ethane phase equilibrium experimental and simulation data cover a much broader pressure range, up to 3500 bar (Figures 6 through 8). Although at 523 and 573 K experimental data indicate a monotonic increase of ethane solubility with pressure,[17] molecular simulation using either of the two models predicts a maximum ethane solubility at ∼500 bar for the MPSC/E−TraPPE model and 1000−1500 bar for the exp-6 model (Figures 6 and 7). A similar behavior is shown by APACT, which predicts maximum ethane solubility at 1000−1200 bar for the temperature range examined. The actual values for the ethane solubility in water are very close for all three models. On the other hand, although SAFT qualitatively agrees with the experimental data, the actual solubility values it predicts are 20−60% higher than the experimental ones.

For the water solubility in ethane at 523 and 573 K, the exp-6 model is in better agreement with the experimental data[17] than the MSPC/E−TraPPE model, as is the case for water in methane. APACT predictions are very close to the experimental data and exp-6 results, whereas SAFT predictions are approximately twice the experimental values.

The phase diagram for water−ethane mixture at 623 K is qualitatively different than it is at lower temperatures. At relatively low pressures, the mutual solubility of the two components increases with pressure and at 680 bar the mixture becomes completely miscible (upper critical solution pressure, UCSP). The mixture remains miscible up to 760 bar, where a lower critical solution pressure (LCSP) appears and the mixture becomes again immiscible. GEMC with the exp-6 model predicts mutual solubilities at low pressure (<500 bar) and high pressure (>1000 bar) that are in good agreement with the experimental data. Simulation in the pressure range 500−1000 bar indicated that the model predicts complete miscibility. One can conclude, therefore, that molecular simulation with an accurate molecular model is able to predict this complex phase behavior.

APACT and SAFT predict that water and ethane are partially miscible over the entire pressure range. SAFT predicts an hourglass behavior, which indicates that the two components are miscible over a small pressure range at higher temperatures. These predictions are due to the fact that both the APACT and SAFT critical temperatures for water are well above the experimental value of 647.1 K.

It is quite remarkable that for both mixtures examined here and for conditions away from the water critical point, APACT

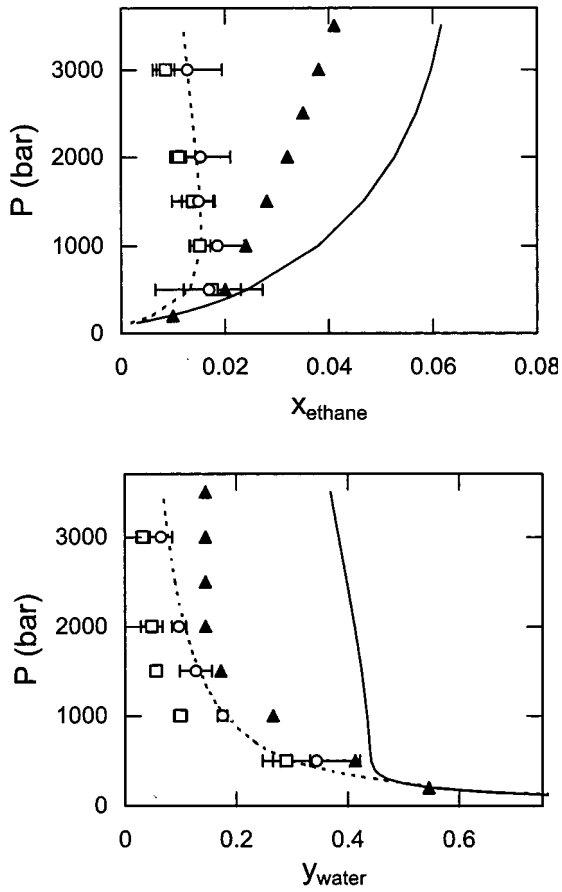

Figure 7. Water−ethane high-pressure phase equilibria at 573 K (top: liquid-phase composition; bottom: vapor-phase composition). Experimental data (solid triangles),[17] GEMC simulation with the MSPC/E−TraPPE model (open squares) and with the exp-6 model (open circles), and EoS predictions from APACT (dashed lines) and SAFT (solid lines).

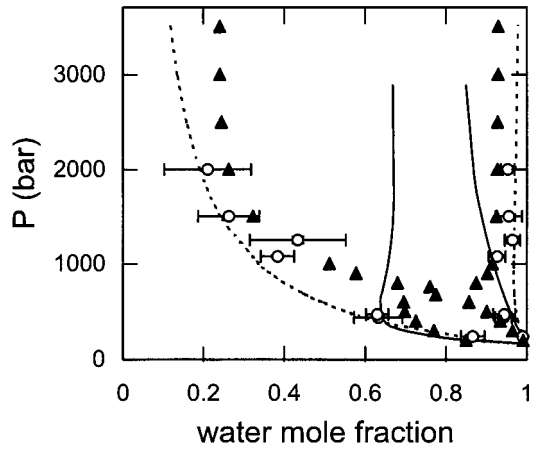

Figure 8. Water−ethane high-pressure phase equilibria at 623 K. Experimental data (solid triangles),[17] GEMC simulation with the exp-6 model (open circles), and EoS predictions from APACT (dashed lines) and SAFT (solid lines).

predictions are in close agreement with the simulation results, unlike SAFT, the predictions of which deviate considerably from simulation. This agreement is more pronounced for the hydrocarbon-rich phase (either methane or ethane). This behavior can be attributed to the fact that APACT accounts for local composition effects through a second-order Lennard−Jones perturbation expansion, dipole−dipole perturbation expansion, and asymmetric mixing rules,[33] whereas SAFT does not.[32] In other words, APACT captures, even approximately, all the interactions described on the molecular level by the different two-body molecular models used in our simulations. The limitations of APACT are its inaccuracy for temperatures close to one of the component's critical point and for mixtures containing chain fluids. It is well known that APACT does not have an accurate chain term. It simply predicts that the chain term of the EoS can be calculated from the Carnahan−Starling expression for hard spheres multiplied by the chain length.[20] As a result, APACT becomes highly inaccurate for mixtures that contain chain molecules such as heavy hydrocarbons.

Conclusions

In this work, the water−methane and water−ethane phase equilibria were examined from approximately room temperature up to the critical point of water. Monte Carlo simulations were compared with literature experimental data and EoS predictions. At relatively low pressure, Henry's law is a convenient way to describe the hydrocarbon solubility in water. The two molecular models used, SPC/E and MSPC/E, were in good agreement with experimental data. As the pressure increases, the mutual solubility increases substantially and the system is best described by the compositions of the two coexisting phases. For these conditions, the GEMC simulation method was used to predict the mixture phase equilibria using the MSPC/E and the exp-6 models. In general, the results were in good agreement with experimental data. However, because the exp-6 model is more accurate than the MSPC/E model in the vicinity of the pure water critical point, water−methane simulations at 603 K were closer to the experimental data using the exp-6 model than the MSPC/E model. Furthermore, the exp-6 model was able to capture the very complex phase behavior of the water−ethane mixture at 623 K where a UCSP and a LCSP are exhibited.

EoS predictions were in relatively good agreement with experimental data only at temperatures well below the critical temperature of pure water. In addition, the EoS tested here were specifically designed for associating fluids. When applied to other types of asymmetric mixtures, for example mixtures of heavy hydrocarbons, they are significantly less accurate.[24] By contrast, molecular simulations of asymmetric hydrocarbon mixtures presented elsewhere[24] are in excellent agreement with experimental data, thus confirming the generality of the approach.

We showed here clearly that molecular simulation is a reliable tool for the calculation of mixture phase equilibria of very dissimilar components such as water and hydrocarbons and for conditions that are difficult to be reached experimentally, such as a few kilobar of pressure. The level of accuracy of potential models for the prediction of pure component properties has a direct effect on the accuracy for mixture predictions. Deviations between simulation and experiment observed in this work can be possibly reduced by including in the potential models explicitly the many body effects, such as polarizability effects, which are nonnegligible for water−hydrocarbon mixtures.[39,40] The price to pay for such an increase in the accuracy of the calculations will be the considerably higher computing time.[40,41]

Acknowledgment. We are grateful to Professor J. I. Siepmann and Professor J. J. de Pablo for providing their manuscripts before publication. The work at Cornell University and the University of Maryland was supported by the National Science Foundation under grant CTS-9509158. Partial financial support

of this project from NATO Collaborative Research Grants Program under grant number CRG 960966 is gratefully acknowledged.

References and Notes

(1) Tsonopoulos, C.; Wilson, G. M. *AIChE J.* **1983**, *29*, 990.
(2) Heidman, J. L.; Tsonopoulos, C.; Brady, C. J.; Wilson, G. M. *AIChE J.* **1985**, *31*, 376.
(3) Brunner, E. *J. Chem. Thermodyn.* **1990,** *22*, 335.
(4) Economou, I. G.; Heidman, J. L.; Tsonopoulos, C.; Wilson, G. M. *AIChE J.* **1997**, *43*, 535.
(5) Panagiotopoulos, A. Z. *Mol. Phys.* **1987**, *61*, 813.
(6) Panagiotopoulos, A. Z. In *Supercritical Fluids−Fundamentals for Application;* E. Kiran and J. M. H. Levelt Sengers, Eds.; Kluwer Academic Publishers: Dordrecht, 1994; p 411.
(7) Mehta, M.; Kofke, D. A. *Chem. Eng. Sci.* **1994,** *49*, 2633.
(8) Spyriouni, T.; Economou, I. G.; Theodorou, D. N. *Macromolecules* **1997**, *30*, 4744.
(9) Jorgensen, W. L.; Chandrasekhar, J.; Madura, J. D.; Impey, R. W.; Klein, M. L. *J. Chem. Phys.* **1983,** *79*, 926.
(10) Berendsen, H. J. C.; Postma, J. P. M.; van Gunsteren, W. F.; Hermans, J. In *Intermolecular Forces*, Pullman, B., Ed.; Reidel: Dordrecht, 1981; p 331.
(11) Berendsen, H. J. C.; Grigera, J. R.; Straatsma, T. P. *J. Phys. Chem.* **1987,** *91*, 6269.
(12) Boulougouris, G. C.; Economou, I. G.; Theodorou, D. N. *J. Phys. Chem. B* **1998,** *102*, 1029.
(13) Errington, J. R.; Panagiotopoulos, A. Z. *J. Phys. Chem. B* **1998**, *102*, 7470.
(14) Smit, B.; Karaborni, S.; Siepmann, J. I. *J. Chem. Phys.* **1995,** *102*, 2126.
(15) Nath, S. K.; Escobedo, F. A.; de Pablo, J. J. *J. Chem. Phys.* **1998,** *108*, 9905.
(16) Martin, M. G.; Siepmann, J. I. *J. Phys. Chem. B* **1998,** *102*, 2569.
(17) Danneil, A.; Toedheide, K.; Franck, E. U. *Chemie-Ing. Techn.* **1967,** *39*, 816.
(18) Sultanov, R. G.; Skripka, V. G.; Yu, N. A. *Zh. Fiz. Khim.* **1972,** *46*, 2160.
(19) Harvey, A. H. *AIChE J.* **1996**, *42*, 1491.
(20) Ikonomou, G. D.; Donohue, M. D. *AIChE J.* **1986**, *32*, 1716.
(21) Huang, S. H.; Radosz, M. *Ind. Eng. Chem. Res.* **1990**, *29*, 2284.
(22) Bernal, J. D.; Fowler, R. H. *J. Chem. Phys.* **1933,** *1*, 515.
(23) Buckingham, R. A. *Proc. R. Soc.* **1938,** *168A*, 264.
(24) Spyriouni, T.; Economou, I. G.; Theodorou, D. N. *Phys. Rev. Lett.* **1998,** *80*, 4466.
(25) Prausnitz, J. M.; Lichtenthaler, R. N.; de Azevedo, E. G. *Molecular Thermodynamics of Fluid-Phase Equilibria*, 2nd ed.; Prentice Hall: Englewood Cliffs, NJ, 1986.
(26) Widom, B. *J. Chem. Phys.* **1963,** *39*, 2808.
(27) Allen, M. P.; Tildesley, D. J. *Computer Simulation of Liquids*; Clarendon Press: Oxford, 1987.
(28) Siepmann J. I. *Mol. Phys.* **1990,** *70*, 1145.
(29) Frenkel, D.; Mooij, G. C. A. M.; Smit, B. *J. Phys. Cond. Matt.* **1992,** *4*, 3053.
(30) de Pablo, J. J.; Laso, M.; Suter, U. W. *J. Chem. Phys.* **1992,** *96*, 2395.
(31) Theodorou, D. N.; Suter, U. W. *J. Chem. Phys.* **1985**, *82*, 955.
(32) Huang, S. H.; Radosz, M. *Ind. Eng. Chem. Res.* **1991**, *30*, 1994.
(33) Economou, I. G.; Peters, C. J.; de Swaan Arons, J. *J. Phys. Chem.* **1995**, *99*, 6182.
(34) Economou, I. G.; Tsonopoulos, C. *Chem. Eng. Sci.* **1997,** *52*, 511.
(35) Vimalchand, P.; Ikonomou, G. D.; Donohue, M. D. *Fluid Phase Equilib.* **1988,** *43*, 121.
(36) Guillot, B.; Guissani, Y. *J. Chem. Phys.* **1993,** *99*, 8075.
(37) Beutier, D.; Renon, H. *AIChE J.* **1978**, *24*, 1122.
(38) Schotte, W. *AIChE J.* **1985**, *31*, 154.
(39) Chialvo, A. A.; Cummings, P. T. *J. Chem. Phys.* **1996,** *105*, 8274.
(40) Kiyohara, K.; Gubbins, K. E.; Panagiotopoulos, A. Z. *Mol. Phys.* **1997,** submitted.
(41) Ahlström, P.; Wallqvist, A.; Engström, S.; Jönsson, B. *Mol. Phys.* **1989,** *68*, 563.